Food Chemistry: X 23 (2024) 101752

Contents lists available at ScienceDirect

Food Chemistry: X

journal homepage: www.sciencedirect.com/journal/food-chemistry-x

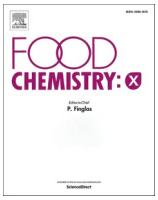

Direct detection of ethyl carbamate in baijiu by molecularly imprinted electrochemical sensors based on perovskite and graphene oxide

Wanqi Zheng [a,b], Mingcai Yao [a,b], Yinjiang Leng [a,b], Kangjie Yu [a,b], Xiongjun Xiao [a,b], Huiling Huang [a,b], Xiao Yu [a,b], Yi Ma [a,b,*], Changjun Hou [a,*]

[a] College of Bioengineering, Sichuan University of Science and Engineering, Yibin 644000, China,
[b] Engineering Technology Research Center of Special Grain for Wine Making, Yibin 644000, China.

ARTICLE INFO

Keywords:
Perovskite
Molecular imprinting
Electrochemical sensor
Ethyl carbamate

ABSTRACT

Ethyl carbamate (EC), a carcinogen commonly found in Baijiu, requires an efficient detection method for quality control and monitoring. This study introduces a novel molecularly imprinted electrochemical sensor for sensitive and selective EC detection. We proposed a simple sol-gel method for the growth of perovskite-structured lanthanum manganate ($LaMnO_3$) on graphene oxide (GO). A non-enzymatic electrochemical sensor was developed by coating a molecularly imprinted polymer synthesized via precipitation polymerization onto the surface of $LaMnO_3$@GO. $LaMnO_3$, with its superior three-dimensional nanocube structure, demonstrated excellent electrocatalytic activity, while the addition of GO provided a large specific surface area. The results indicate that the developed sensor exhibits exceptional recognition ability and electrochemical activity, which is attributed to the high affinity of $LaMnO_3$@GO@MIP for EC. The sensor displays a broad linear range from 10 to 2000 μM, with a detection limit as low as 2.18 μM and long-term durability of 28 days. Notably, it demonstrates excellent selectivity, reproducibility, and stability even under different interference conditions. The sensor was successfully used to determine EC in real Baijiu samples. Overall, the sensor has broad application prospects for detecting trace contaminants in the field of food safety.

1. Introduction

Ethyl carbamate (EC) is a genotoxic carcinogen present in fermented foods and alcoholic beverages, posing serious health risks (Wei et al., 2021). It is associated with tumors in various tissues (Deng et al., 2023) and is challenging to remove once absorbed (Xia et al., 2022). According to the Codex Committee on Food Additives (CCFA), alcoholic beverages are the primary source of human EC intake (Shalamitskiy et al., 2023), with the Food and Agriculture Organization of the United Nations (FAO) setting a maximum allowable content of 20 μg/L in 2002 (Zhou et al., 2021). Current detection methods such as gas chromatography–mass spectrometry (GC–MS) (Ma et al., 2022), multidimensional gas chromatography–mass spectrometry (MDGC–MS) (Tu et al., 2018), high performance liquid chromatography-fluorescence detection (HPLC-FLD) (Aguilera Ojeda et al., 2019), and ultra performance liquid chromatography-mass spectrometry (UPLC-MS) (Lee et al., 2017) are highly accurate but involve complex procedures and costly equipment, which limits their feasibility for rapid on-site detection. Recent advances include immunoassays using antibodies, enzymes, and aptamers as specific recognition receptors (Fu et al., 2021), as well as fluorescence (Luo et al., 2018; Wei et al., 2021), Raman spectroscopy (Qi et al., 2018), colorimetric (Xia et al., 2022), and electrochemical technologies (Wu et al., 2021) for EC detection. Although these techniques offer high accuracy and sensitivity, they are often associated with high costs and stringent storage conditions. Given these limitations, there is an urgent need for real-time, rapid, and accurate EC detection using biomimetic receptor technology.

Molecularly Imprinted Polymers (MIPs) are synthetic polymers with distinctive molecular recognition capabilities that have recently gained prominence. They are prepared by *co*-polymerizing a template molecule with a functional monomer under controlled conditions. After polymerization, the target molecule is removed, leaving a specific spatial structure formed by the functional monomer (Scheller et al., 2019). The imprinted cavity retains both the structure of the target molecule and the necessary molecular interactions for target recognition, including hydrogen bonding, electrostatic attraction, and hydrophobic areas

* Corresponding authors at: College of Bioengineering, Sichuan University of Science and Engineering, Yibin 644000, China.
E-mail addresses: zhangyer2008@suse.edu.cn (Y. Ma), houcj@cqu.edu.cn (C. Hou).

https://doi.org/10.1016/j.fochx.2024.101752
Received 23 May 2024; Received in revised form 23 July 2024; Accepted 17 August 2024
Available online 22 August 2024

(Mintz Hemed et al., 2023). MIPs serve as ideal alternatives to antibodies and aptamers due to their advantages of rapid synthesis, simple preparation, low cost, and exceptional chemical and thermal stability (Meng et al., 2024). Notably, MIPs display highly selective properties due to their pore structure, which is tailored to the target substance, enabling them to selectively re-recognize and adsorb target molecules (Fu et al., 2019). Consequently, MIPs can be used to recognize and modify compounds on electrode surfaces to capture and detect EC. Electrochemical sensors that employ molecular imprinting as a recognition response molecule offer benefits such as simple sample pretreatment, high sensitivity, strong specificity, low operational cost, ease of storage, miniaturization, and automation (Xing et al., 2023). This approach combines the specific recognition capabilities of MIPs with the high sensitivity of electrochemical detection, making it an optimal strategy for detecting EC.

Perovskite is a novel material characterized by its distinctive crystal structure. Its chemical formula is generally ABX_3, in which rare earth or rare earth metal atoms are situated at the center of the cell (A position), transition metal atoms occupy the corners of the cell (B position), and halogen or oxygen anions are located at the center of each face of the cell (X position). Perovskite-type materials are known for their remarkable physical and chemical properties, including tunable redox properties, excellent metal-oxygen ion conductivity, superior reactive electronic structure, high electrocatalytic activity, and long-term chemical stability (Koventhan et al., 2023). These properties make perovskite materials ideal for the development of EC molecularly imprinted sensors. ABX_3-type perovskite-based electrode materials have demonstrated effectiveness in sensing applications using various electrochemical methods, notably cyclic voltammetry and square-wave voltammetry, on glassy carbon electrodes (GCE) and screen-printed electrodes (SPCE) (George et al., 2020). The sensors constructed using these materials have demonstrated impressive detection performance. Among these materials, $LaMnO_3$ is a highly conductive p-type semiconductor with exceptional oxygen reduction reaction activity, offering distinctive electronic and catalytic properties for sensor applications (Zhang & Yi, 2018). However, perovskite materials often have large particle sizes and limited specific surface areas. Additionally, the high calcination temperatures required for their synthesis can result in reduced conductivity of perovskite, limiting the broader application of perovskite-type materials in rapid detection (Mohseni et al., 2024). To address this issue, various nanomaterials, including metal-based (Zhu et al., 2022) and carbon-based nanomaterials (Koventhan et al., 2023) can be employed to enhance the sensitivity of perovskite-type molecularly imprinted electrochemical sensors. Among these materials, graphene oxide (GO) is a two-dimensional planar sheet with a honeycomb structure and sp^2 hybridization. Due to its large surface area, exceptional electrical conductivity, strong chemical stability, and outstanding thermal and mechanical properties, GO has a wide range of potential applications in electrochemical sensors (Mani et al., 2023). Additionally, GO is highly hydrophilic and water-soluble, and its numerous oxygen functional groups and aromatic rings enhance interactions with target substances (Ma et al., 2023). Furthermore, increasing the electrode surface area can increase the number of active sites available for the immobilization of MIPs, thereby improving the sensitivity of molecularly imprinted sensors (Lai et al., 2023). Consequently, integrating GO nanomaterials with perovskites and developing molecularly imprinted sensors is an effective approach to combine high conductivity, large specific surface area, and high selectivity.

Given the limited electrochemical activity of EC, we propose for the first time a perovskite-based molecularly imprinted electrochemical sensor for its direct and sensitive detection (Scheme 1). Using the sol-gel method, we grew perovskite $LaMnO_3$ on the flaky nanostructure of GO. Surface molecularly imprinting polymerization was then performed with $LaMnO_3$@GO as the carrier material. The electrodes were constructed by drop-casting $LaMnO_3$@GO@MIP onto the surface of a bare GCE, creating a new working electrode for EC monitoring. This sensor exhibits superior stability, high sensitivity, and selectivity for detecting EC in Baijiu samples.

2. Materials and methods

2.1. Reagent

Graphite powder, potassium permanganate, concentrated sulfuric

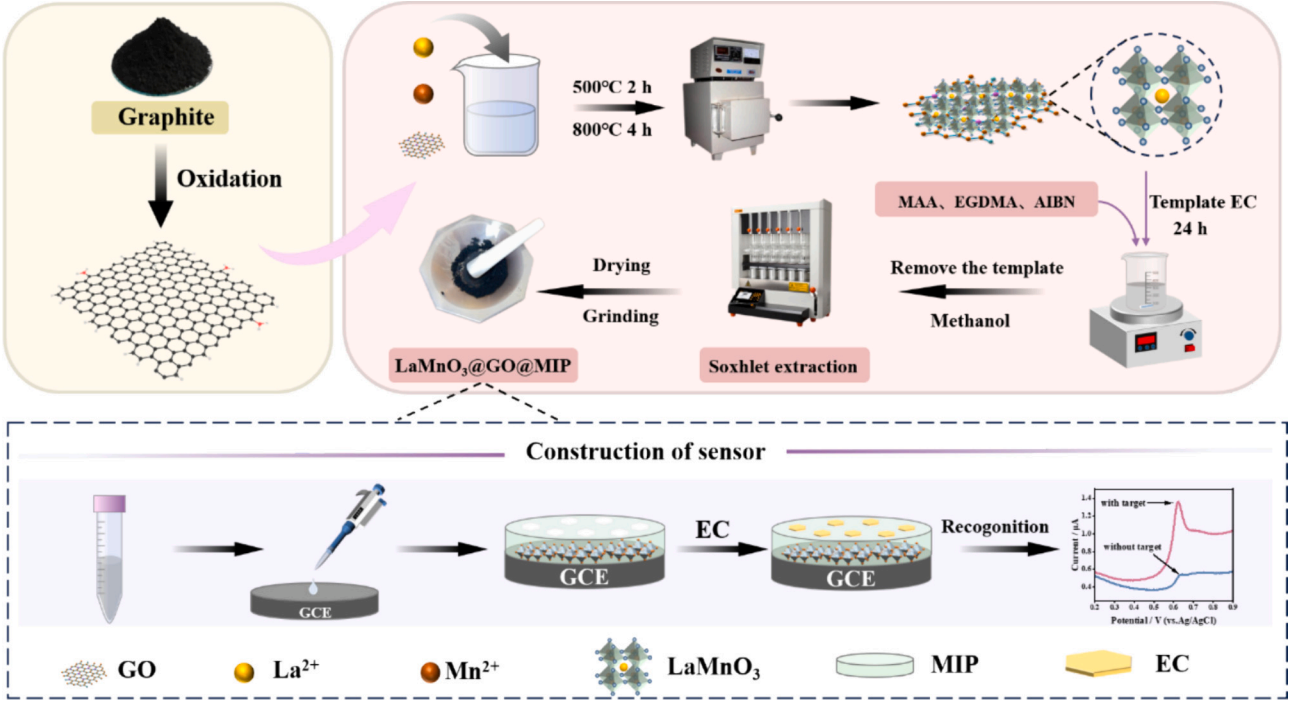

Scheme 1. Schematic illustration of synthesis of the $LaMnO_3$@GO@MIP composite and the electrochemical sensing procedure for ethyl carbamate.

acid, lanthanum nitrate hexahydrate, manganese nitrate hexahydrate, citric acid, potassium ferricyanide, ethyl carbamate (EC), methacrylic acid (MAA), ethylene glycol dimethacrylate (EGDMA), azobisisobutyronitrile (AIBN), 2-aminophthalic acid, *N*-methylurethane, isoprocarb, 2-amino-3-fluorobenzoate, methyl 2-aminothiazole-5-carboxylate, ethyl benzoate, ethyl 2-methylbutyrate, urea, ammonium chloride, ammonium sulfate purchased from Chengdu Platinum Strontium Titanium Biotechnology Co., LTD. (Chengdu, China). All reagents used in this study were of analytical grade. Strong-flavor Baijiu was purchased from local markets (Yibin, China). Ultrapure water (≥18.2 5 MΩ cm) was used throughout the experiment.

2.2. Instrument

The electrochemical workstation (CHI 660 E, Chenhua Instrument Co., Ltd., China) was used for all electrochemical measurements. The platinum electrode (Pt), Ag/AgCl electrode and glassy carbon electrode (GCE, φ = 3 mm) were used as the auxiliary electrode, reference electrode and working electrode of the three-electrode test system. Scanning electron microscopy (SEM, Nova 400, Thermo Fisher Technologies, USA) and transmission electron microscopy (TEM, FEI Technology F20, FEI Corporation, USA) were used to characterize the morphological and structural characteristics of the materials. The X-ray photoelectron spectroscopy (XPS, Thermo Nexsa, Thermo Fisher Technologies, USA) was used to characterize the elemental composition of materials. Fourier transform infrared spectroscopy (FTIR, Thermo Nicolet iS5, Thermo Fisher Technologies, USA) was used to detect functional groups in materials. The X-ray diffraction (XRD, Ultima IV, Rigaku Beijing Corp., China) was used to determine the crystal structure of the material.

2.3. Synthesis of $LaMnO_3$@GO

GO was synthesized by the modified Hummers method (Balaji et al., 2019). $LaMnO_3$@GO was synthesized by the modified sol-gel method (Sfirloaga et al., 2023). 2.8 mmol of lanthanum nitrate and 2.8 mmol of manganese nitrate were dissolved in an aqueous solution. After stirring for 30 min with a constant temperature magnetic mixer at 40 °C, 5.6 mmol of citric acid was added and the mixture was continued at 60 °C for 120 min. 0.168 g of GO powder was then added, followed by ultrasonic dispersion for 1 h. The resulting clarified sol was placed in an oven at 10 5 °C, and gradually formed a brown dry gel. After the sample was dried, the oven temperature was increased to 180 °C for 30 min. At this point, the dry gel spontaneously combusted, forming a loose black substance. The obtained black sample was ground and put into a muffle furnace, calcined at 500 °C for 2 h, and then heated to 800 °C for 4 h. After the sample was cooled down to room temperature, the powder $LaMnO_3$@GO was obtained. For comparison, pure $LaMnO_3$ powder was prepared under the same conditions.

2.4. Synthesis of $LaMnO_3$@GO@MIP(NIP)

Molecularly imprinted polymers were synthesized as described in the literature, with slight modifications (Han et al., 2023). EC (0.0 5 mmol) was dispersed in 10 mL methanol, and then MAA (0.3 mmol) was added to the mixture under continuous agitation of nitrogen. Then, EGDMA (0.5 mmol) and AIBN (20 mg) were slowly mixed in a stirrer after 30 min, followed by the addition of 50 mg of $LaMnO_3$@GO and vigorous shaking in a water bath at 60 °C for 24 h. Template molecules were removed from the molecularly imprinted polymer on $LaMnO_3$@GO by Soxhlet extraction and washing with methanol for 36 h. When no EC is detected in the washing solution by the GC-MS method, washing is complete. After drying and grinding, a gray solid powder $LaMnO_3$@GO@MIP was obtained. The $LaMnO_3$@GO@NIP polymer without EC was synthesized in the same way as the control sample.

2.5. Preparation of $LaMnO_3$@GO@MIP/GCE electrode

The preparation procedure of $LaMnO_3$@GO@MIP/GCE electrode was according to the method in the literature and modified appropriately (Yao et al., 2024). Prior to modification, the bare GCE was polished with 0.3 and 0.0 5 μm alumina polishing powders for 3 min until the surface presented a smooth mirror, then rinsed with ethanol and ultrapure water, dried and set aside. 20 mg of $LaMnO_3$@GO@MIP was dispersed in 1 mL of ethanol and ultrasonicated for 30 min, resulting in a $LaMnO_3$@GO@MIP suspension with a concentration of 20 mg/mL. 6 μL of $LaMnO_3$@GO@MIP composite was coated onto the pretreated GCE surface to complete the construction of the $LaMnO_3$@GO@MIP/GCE sensor. For comparison, $LaMnO_3$, GO, $LaMnO_3$@GO and $LaMnO_3$@GO@NIP modified GCE were prepared using the same procedure with the same amount of composite modification.

2.6. Electrochemical measurements

For electrochemical studies, 5.00 mM $[Fe(CN)_6]^{3-/4-}$ (including 1 M KCl) was used as a redox probe and the modified electrode was characterized by electrochemical impedance spectroscopy (EIS) (Guo et al., 2018). Electrochemical measurements were performed in phosphate buffers containing EC (0.01 M PBS, pH 7.5) by cyclic voltammetry (CV) and square wave voltammetry (SWV). CV has a potential range of −0.2 to 1.2 V at a sweep rate of 50 mV s^{-1}, and SWV has a potential range of 0 to 0.9 V with an amplitude, frequency and pulse period of 0.02 5 V, 1 5 Hz and 2 s, respectively. The generated oxidation peak current difference (ΔI) is defined as the detection response signal of the constructed sensor. ΔI represents the difference between the oxidation peak current (Ip) and the baseline current (Ib), reflecting the change in current before and after the redox reaction.

2.7. Analysis of EC in actual samples

In order to verify the accuracy of $LaMnO_3$@GO@MIP/GCE sensor in the actual sample detection, Strong-flavor Baijiu was selected as the actual sample. This method does not require complex pre-processing. After the samples were diluted 1000 times with ethanol, the concentrations of 10, 50, 100, 200 and 500 μM EC were added, and the recovery of EC in the standardized samples was calculated (Han et al., 2022). The gas chromatography–mass spectrometry (GC–MS) was used to verify the accuracy of the results (Ma et al., 2022).

3. Results and discussion

3.1. Characterization of $LaMnO_3$@GO@MIP

The surface morphology of the produced nanomaterials was characterized using scanning electron microscopy (SEM) and transmission electron microscopy (TEM) (Fig. 1). The $LaMnO_3$ sample (Fig. 1a) consisted of regularly distributed nanotubes, with the solid particles evenly dispersed and an average particle size of 69.86 nm, without clumping. The synthesized GO exhibited a typical flaky two-dimensional structure, providing additional adsorption binding sites. The SEM image of the $LaMnO_3$@GO composite revealed that the particle size was approximately 59.49 nm after cladding $LaMnO_3$ on top of GO, resulting in a porous and tightly agglomerated appearance. The porous structure enhances the diffusion of electrolyte ions and increases the availability of active catalytic sites (Mohseni et al., 2024). Following molecularly imprinted modification, the material exhibited an irregular morphology, with the agglomeration phenomenon eliminated. The surface of $LaMnO_3$@GO@MIP (Fig. 1d) became rough and porous, indicating an improved three-dimensional structure. The molecularly imprinted surface features visible concave voids that provide numerous imprinting sites for molecular imprinting, thereby enhancing the adsorption of EC molecules. For comparison, the non-imprinted polymers

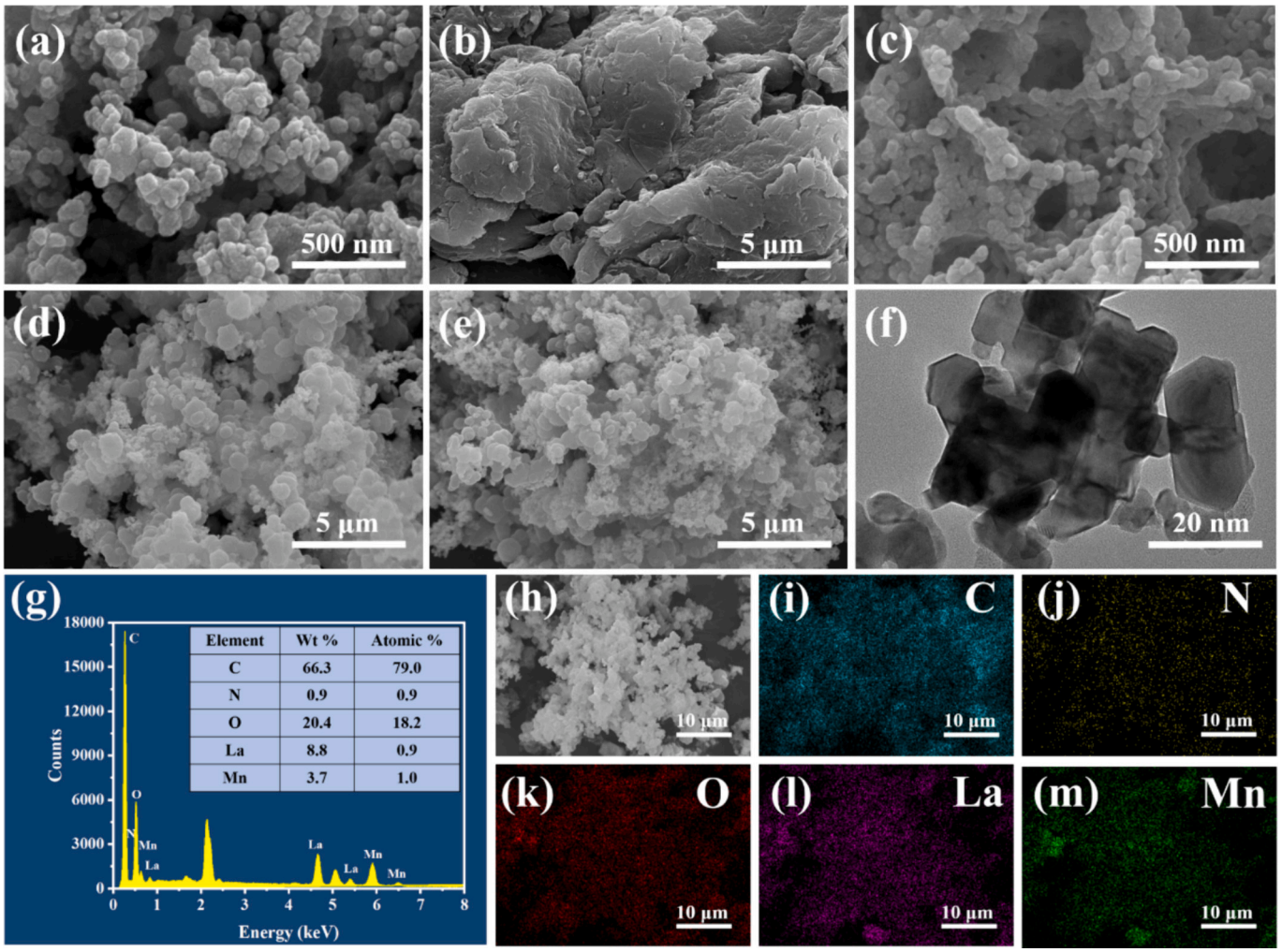

Fig. 1. SEM image of **(a)** $LaMnO_3$, **(b)** GO, **(c)** $LaMnO_3$@GO, **(d)** $LaMnO_3$@GO@MIP and **(e)** $LaMnO_3$@GO@NIP; **(f)** TEM image of $LaMnO_3$@GO@MIP; **(g)** SEM-EDS spectra of $LaMnO_3$@GO@MIP; **(h)** prepared $LaMnO_3$@GO@MIP element maps, including **(i)** C, **(j)** N, **(k)** O **(l)**La and **(m)**Mn.

$LaMnO_3$@GO@NIP were also characterized by SEM. As shown in Fig. 1e, $LaMnO_3$@GO@NIP displays a similar morphology to $LaMnO_3$@GO@MIP. However, non-imprinted polymers exhibit a more condensed arrangement and a greater tendency to aggregate than imprinted polymers. This was due to the absence of template EC during synthesis and the lack of hydrogen bonding between MAA and EC, which affected the growth of the cross-linked polymer nuclei and resulted in the formation of block polymers (Liang et al., 2017).

Energy-dispersive X-ray spectroscopy (EDS) spectra of the $LaMnO_3$@GO@MIP material were obtained from the specific location shown in Fig. 1g for further analysis. The spectrum analysis revealed the presence of C, O, N, La, and Mn in the synthesized material, with these elements uniformly distributed throughout the composite material. The small amount of N detected was likely due to the polymerization of the molecularly imprinted material. The atomic ratio of La to Mn was approximately 1:1, which is consistent with the theoretical value, confirming that the produced materials were synthesized at the intended ratio.

X-ray photoelectron spectroscopy (XPS) was employed to determine the surface composition and chemical states of $LaMnO_3$@GO@MIP. Fig. 2a shows the XPS survey spectrum of the as-synthesized $LaMnO_3$@GO@MIP, calibrated by the C 1 s peak. The scanning spectrum indicates the presence of C, O, La, Mn, and N, consistent with the EDS findings. Fig. 2b illustrates the deconvolution of the C 1 s peak into three distinct peaks at 284.80, 286.61, and 288.67 eV, corresponding to C—C, C—O, and C═O bonds, respectively (Han et al., 2019). The oxygen peaks in the O 1 s spectrum of Fig. 2c were analyzed and found to consist of three distinct peaks at 529.07, 531.68, and 533.29 eV. These peaks correspond to the presence of metal-oxygen, C—O, and C═O bonds. Fig. 2d illustrates the La 3d spectra of $LaMnO_3$@GO@MIP. In this region, the spin-orbital components of La are distinguishable, with each component further divided by multiplet splitting. The peaks observed at 833.81 and 837.92 eV correspond to the La $3d_{5/2}$ orbital splitting, whereas the La $3d_{3/2}$ orbital is represented by two peaks at 8 50.41 and 8 54.52 eV (Zhang et al., 2024). Furthermore, the distinct 16.6 eV distance between the La $3d_{5/2}$ and La $3d_{3/2}$ peaks indicates the presence of La^{3+} ions (Song et al., 2020). The peaks at 641.13 and 6 52.68 eV in the Mn 2p spectrum (Fig. 2e) correspond to Mn^{3+}, whereas the peaks at 643.04 and 6 54.44 eV represent Mn^{4+}. These results suggest that the manganese in $LaMnO_3$ is predominantly present as Mn^{3+} and Mn^{4+}. The Mn^{3+}/Mn^{4+} ratio is 0.68/0.32, indicating that Mn^{3+} is the predominant species. Fig. 2f shows the N 1 s spectrum, with a peak at 399.24 eV corresponding to the N—H bond (Han et al., 2023), which suggests the presence of AIBN during molecularly imprinted polymerization. These results confirm the successful preparation of $LaMnO_3$@GO@MIP.

To verify the functional groups of the different nanomaterials, the infrared spectra of $LaMnO_3$, GO, $LaMnO_3$@GO, $LaMnO_3$@GO@MIP, and $LaMnO_3$@GO@NIP were analyzed by Fourier transform infrared spectroscopy (FTIR). As shown in Fig. 3a, all nanomaterials combined with $LaMnO_3$ exhibited a distinct peak within the range of

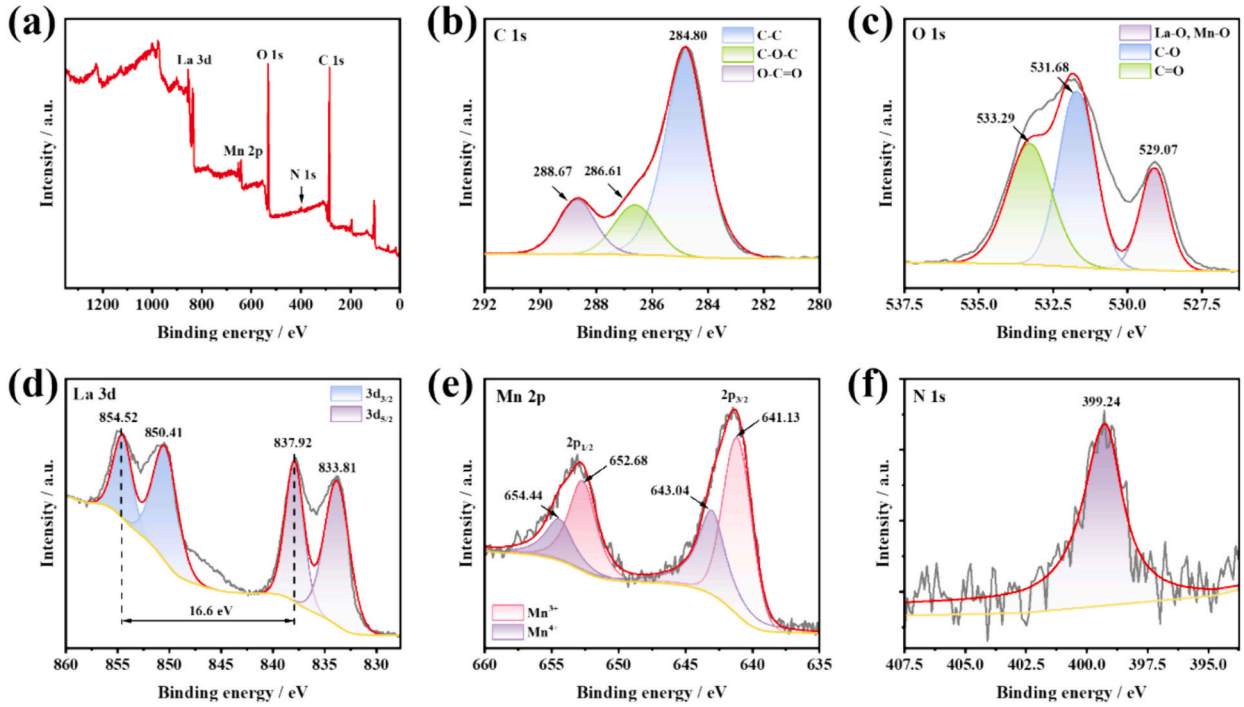

Fig. 2. **(a)** XPS spectra of $LaMnO_3$@GO@MIP; High-resolution spectra of **(b)** C 1 s, **(c)** O 1 s, **(d)** La 3d, **(e)** Mn 2p, **(f)** N 1 s.

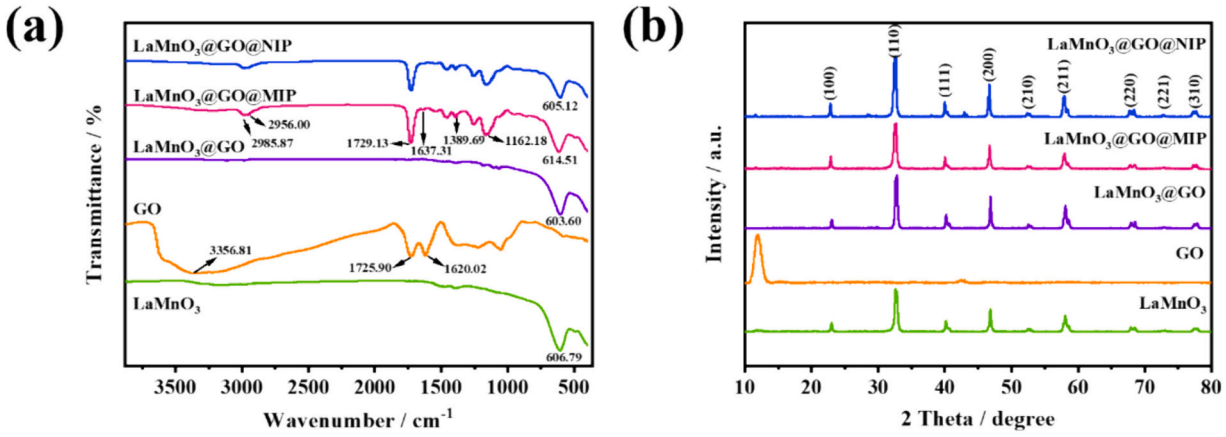

Fig. 3. **(a)** FT-IR spectrum; **(b)** XRD pattern.

603.60–614.51 cm^{-1}. This peak is likely associated with the telescopic vibration of the metal-oxygen link in $LaMnO_3$, demonstrating the successful incorporation of $LaMnO_3$ materials (Sfirloaga et al., 2023). GO contains additional oxygen-containing groups, with a broad hydroxyl vibration peak at 33 56.81 cm^{-1}, and a peak at 172 5.90 cm^{-1} attributed to the asymmetric C—O stretching vibration in -COOH on the GO surface. The peak at 1620.02 cm^{-1} confirms the C—C stretching vibration and the presence of sp^2 C—C bonds, indicating the successful oxidation of graphene. (Chen et al., 2024; Mani et al., 2023). After the introduction of GO, the hydroxyl peaks in the $LaMnO_3$@GO structure disappeared, indicating that most of the hydroxyl groups were removed during the composite preparation. Compared with the FTIR spectra, the modified material by molecular imprinting exhibited characteristic peaks for $-CH_3$ stretching vibrations at 298 5.87 cm^{-1} and 29 56 cm^{-1}. The bending vibration of $-CH_3$ at 1389.69 cm^{-1} confirms the presence of the $-CH_3$ functional group in the polymer. The peak at 1729.13 cm^{-1} corresponds to the distinctive peak of the carbonyl C═O stretching vibration, while the peak at 1637.31 cm^{-1} indicates the presence of the C═C functional group. The signal at 1162.18 cm^{-1} is specifically associated with the C − O bond in the ester group of EGDMA (Han et al., 2023). The presence of functional groups such as -CH_3, C═O, and C—O, along with the hydroxyl −OH indicated by the broad peak at 3000 cm^{-1}, suggests that the functional monomer methacrylic acid (MAA) was successfully attached to the surface of $LaMnO_3$@GO during the molecularly imprinted modification process (Elhachem et al., 2023; Li et al., 2020). The spectra of $LaMnO_3$@GO@MIP and $LaMnO_3$@GO@NIP are highly similar, which can be attributed to the fact that the predominant peaks in both spectra originate from the cross-linker EGDMA and the functional monomer MAA.

The final form of the material was analyzed for its composition and crystal structure using X-ray diffraction (XRD), as shown in Fig. 3b. The GO material exhibited a distinct (001) diffraction peak at an angle of 2θ = 11.7 5°, corresponding to a crystal plane spacing of 0.7 5 nm. This spacing was larger than that of graphite (0.34 nm) and was attributed to the presence of hydroxyl, carboxyl, epoxide, and other oxygen-containing groups formed during the oxidation process (Chen et al.,

2024). The typical diffraction peak positions of the prepared $LaMnO_3$ were in good agreement with the standard $LaMnO_3$ spectrum obtained from CPDS card No. 7 5–0440. The characteristic peaks of the sample were observed at $2\theta = 22.90°$, 32.61°, 40.22°, 46.79°, 52.71°, 58.19°, 68.32°, 73.11°, and 77.78°, corresponding to the crystal faces (100), (110), (111), (200), (210), (211), (220), (221), and (310), respectively (Deshmukh et al., 2023). No additional impurity peaks were detected, indicating that the $LaMnO_3$ samples generated are pure. The presence of strong and sharp diffraction peaks indicates that the products exhibit a well-defined crystalline structure. Furthermore, the introduction of GO into $LaMnO_3$ did not alter the crystal structure of $LaMnO_3$, and the characteristic GO peak at 11.7 5° disappeared, confirming the successful incorporation of $LaMnO_3$ nanoparticles onto the GO surface (Mani et al., 2023). After molecularly imprinted modification, the diffraction peaks were compared with the standard $LaMnO_3$ spectra, revealing a high degree of peak matching, which confirms the successful preparation of $LaMnO_3$@GO@MIP materials.

3.2. Optimization of experimental conditions

To optimize the performance of the $LaMnO_3$@GO@MIP/GCE sensor, the response signal ΔI was used to optimize various factors. These factors include the molar ratio of template molecules to functional monomers, the molar ratio of template molecules to EGDMA, the addition of AIBN, the incorporation of $LaMnO_3$@GO, the pH of the buffer solution, and the amount of coating material. Fig. S1 shows the effect of various inspection conditions on the performance of the sensor.

The data presented in Fig. S1a shows the ΔI values for various ratios of EC to MAA concentrations. The electrochemical signal of the sensor varied with the molar ratio of the template molecule EC to the MAA. As the molar ratio of the template to monomer increased from 1:1 to 1:6, the oxidation peak current difference steadily increased. The results suggest that the imprinting spot is affected by the ratio of template to monomer. Excessive numbers of template molecules can lead to their aggregation, resulting in the formation of excessively large imprinting cavities during polymerization. This aggregation weakens the binding between the cavities and templates, thereby impairing the effective capture of template molecules and reducing the sensing performance. However, further increasing the molar ratio of EC to MAA results in a decrease in ΔI. This phenomenon occurs because an excess of functional monomers in solution can lead to their self-association, creating numerous nonspecific binding sites that reduce the recognition ability of the target molecule (Fu et al., 2019). Therefore, the optimal ratio for controlling the template-to-monomer ratio was 1:6.

The concentrations of the crosslinker and initiator directly influence the binding ability of the template molecule EC to functional monomers. Insufficient concentration can hinder the stable polymerization of the template molecule and functional monomer, thereby altering the imprinting cavity. Conversely, excessive concentration leads to the formation of rigid structures with steric hindrance, resulting in polymers with excessive mechanical properties. This impedes the removal of the template and the formation of the cavity necessary for selective adsorption, ultimately reducing the specific recognition ability of the target molecule. Fig. S1b illustrates the effect of the ratio of EC to EDGMA on ΔI. The difference in electrode current increased significantly as the concentration of the crosslinker increased, reaching a peak value when the molar ratio of EC to EDGMA was 1:10. Further increases in the crosslinker concentration led to a notable decrease in the current signal. Fig. S1c examines the impact of varying the amount of AIBN initiator on the sensing current. The results revealed that the magnitude of ΔI was highest when AIBN was introduced at a dosage of 5 mg. An increase in the initiator dose beyond this level results in a reduction in ΔI. Consequently, the optimal ratio of template molecules to EGDMA was determined to be 1:2 5, with the AIBN additive quantity fixed at 5 mg.

Fig. S1d examines the effect of the quantity of $LaMnO_3$@GO on the sensing current during molecular imprinting. The addition of $LaMnO_3$@GO material led to a gradual increase in the oxidation peak current difference, peaking at 50 mg. Beyond this value, the difference in oxidation peak current decreases significantly with increasing addition amount. Therefore, 50 mg was chosen as the optimal amount of $LaMnO_3$@GO composite material for the molecular imprinting process.

The pH value affects both proton transfer in the redox process and the interaction between the electrode modification material and the measured item. Additionally, it influences the imprint recognition capacity of the MIP sensor. Therefore, the impact of pH on the oxidation of $LaMnO_3$@GO@MIP was investigated using a 0.01 M PBS solution with pH values ranging from 5.0 to 9.0 (Fig. S1e). The results revealed that the oxidation peak current difference reached its maximum value at pH 7.5 and decreased with further increases in pH. Consequently, a PBS solution with pH 7.5 was selected as the supporting electrolyte for all experiments.

The amount of $LaMnO_3$@GO@MIP coating on the GCE is a critical factor in determining the sensor sensitivity. Fig. S1f illustrates the electrochemical response currents of the modified electrodes with various coating levels. As the coating amount increased from 2 μL to 6 μL, the oxidation peak current difference progressively increased. Insufficient coating results in inadequate coverage of the GCE surface by $LaMnO_3$@GO@MIP nanomaterials, leading to fewer electron-transfer pathways and weakened electrocatalytic performance, resulting in a lower current response. With 6 μL of the material applied to the GCE surface, the electrode surface was fully covered, and the response current reached its maximum value. This result occurred due to the increased number of effective imprinted cavities on the electrode surface, which enhances the ΔI value. However, further increasing the coating amount decreased the current response. At this stage, excessive stacking of $LaMnO_3$@GO@MIP materials occurs, which interferes with each other, and obstructs EC binding to the imprinted cavities and electron transfer from the electrode surface, thereby reducing the electrocatalytic efficiency. Consequently, 6 μL of the nanomaterial modification solution was applied to the electrode surface to prepare the $LaMnO_3$@GO@MIP modified electrode for subsequent electrochemical experiments.

3.3. Characterization of electrode modification

Cyclic voltammetry (CV) is a valuable technique for analyzing electron movements on modified electrodes. To evaluate the electrochemical properties of $LaMnO_3$@GO@MIP/GCE, several modified electrodes were analyzed using CV in a solution containing 1.00 mM EC (0.01 M PBS, pH 7.5). The results of the CV analysis of bare GCE, GO/GCE, $LaMnO_3$/GCE, $LaMnO_3$@GO/GCE, $LaMnO_3$@GO@NIP/GCE, and $LaMnO_3$@GO@MIP/GCE are depicted in Fig. 4a. Notably, no redox peaks were observed for GCE and GO/GCE in the EC solution. The CV curves of $LaMnO_3$/GCE exhibit a pair of redox peaks for $LaMnO_3$/GCE in the EC solution. The $LaMnO_3$@GO/GCE exhibited a more rapid electron transfer mechanism and a significant enhancement in the redox peak current compared to the $LaMnO_3$/GCE. These results indicate that incorporating GO into the sensor improves conductivity and increases EC oxidation. The peak currents of $LaMnO_3$@GO@MIP/GCE were larger than those of the other modified electrodes, demonstrating faster electron movement on the electrode surface. This enhancement can be attributed to the imprinted cavities provided by molecular imprinting, which facilitate the oxidation of EC on the sensor surface. However, the formation of a nonconductive imprinted film on the surface of the $LaMnO_3$@GO@NIP-modified electrode resulted in a weaker redox pair due to the absence of complementary sites. These findings confirm that the incorporation of GO and $LaMnO_3$ into the MIP/GCE construct results in a gradually increasing peak current.

The electrocatalytic behavior of bare GCE electrodes modified with GO, $LaMnO_3$, $LaMnO_3$@GO, $LaMnO_3$@GO@NIP, and $LaMnO_3$@GO@MIP was investigated using EIS. This analysis employed 5.00 mM [Fe

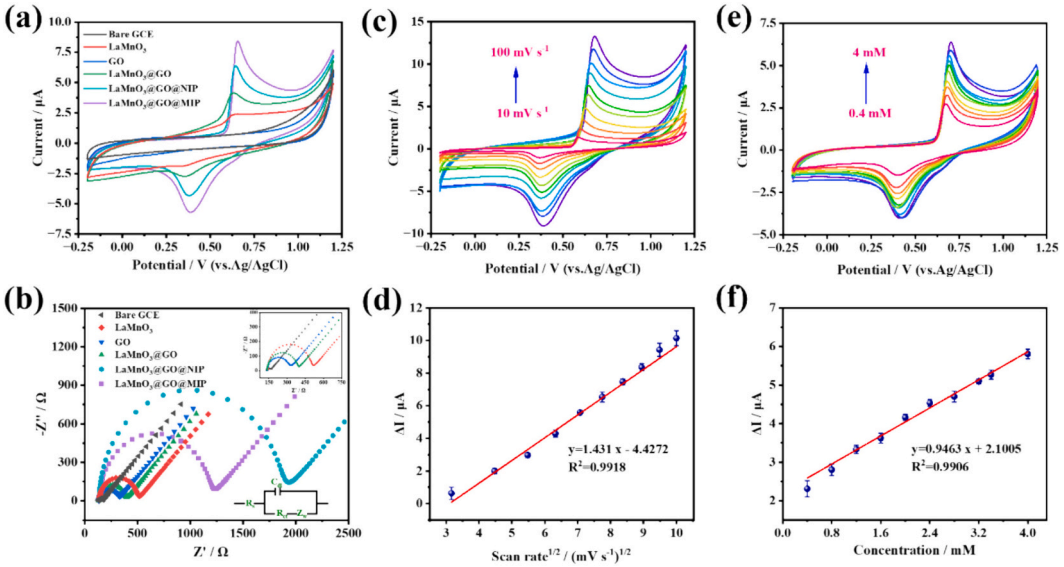

Fig. 4. **(a)** CV curves of various electrodes in the presence of 1 mM EC in 0.01 M PBS, pH 7.5; **(b)** Nyquist plots of various electrodes in the presence of 5 mM $[Fe(CN)_6]^{3-/4-}$ in 0.1 M KCl solution; **(c)** CV curves of $LaMnO_3$@GO@MIP/GCE at different scan rates in the presence of 1 mM EC in 0.01 M PBS, pH 7.5; **(d)** Corresponding fitting of the oxidation peak current difference and scanning rate; **(e)** CV curves of $LaMnO_3$@GO@MIP/GCE in 0.01 M PBS solution containing different concentrations of EC (0.4–4 mM) at a scan rate of 50 mV s^{-1}; **(f)** Corresponding fitting of the oxidation peak current difference and concentrations of EC.

$(CN)_6]^{3-/4-}$ as a redox probe and 0.1 M KCl as the supporting electrolyte. Fig. 4b displays the Nyquist plots of the EIS data recorded from the electrodes over the frequency range of 0.01–100,000 Hz. At both high and low frequencies, the EIS spectral lines reflect the $[Fe(CN)_6]^{3-/4-}$ electronic charge-transfer process and mass-transfer limitation processes (Mani et al., 2023). The results of the AC impedance spectra indicate that the bare electrode exhibited a small peak around 31.8 Ω, which appeared nearly straight, indicating that the bare electrode was well polished. When the electrode was modified with $LaMnO_3$, the charge transfer resistance (R_{ct}) of the electrode was 3 57 Ω. The GO-modified GCE exhibited a lower semicircular curve and charge transfer resistance (176.5 Ω) compared to $LaMnO_3$/GCE. After modification with GO, the R_{ct} decreased due to the highly extended surface area and excellent conductivity of GO. Consequently, the R_{ct} (24 5.2 Ω) of $LaMnO_3$@GO/GCE was intermediate, thereby enhancing the sensor performance. Following further modification of the electrodes by MIP and NIP membranes, the semicircular portions and charge transfer resistance values of $LaMnO_3$@GO@MIP/GCE and $LaMnO_3$@GO@NIP/GCE significantly increased (1038 and 1710 Ω). The observed increase can be attributed to the low conductivity of the molecularly imprinted polymers. MIPs have more 3D-imprinted cavities, providing more active center sites and lower charge-transfer resistance (You et al., 2018).

Furthermore, to evaluate the kinetic properties of the electrochemical redox reaction of EC on modified electrodes, the impact of scanning speeds ranging from 10 mV s^{-1} to 100 mV s^{-1} on the oxidation process was examined using a solution of 0.01 M PBS (pH 7.5) containing 1 mM EC. As shown in Fig. 4c, the anodic current of the EC is proportional to the square root of the scanning rate ($v^{1/2}$) in the range of 10 to 100 mV s^{-1}. An increase in the scanning rate resulted in a positive shift in the anodic peak. The graph in Fig. 4d illustrates the linear correlation between the oxidation peak current difference and the square root of the scanning rate ($v^{1/2}$), which is mathematically expressed as ΔI (μA) = 1.431 $v^{1/2}$(mV s^{-1}) – 4.4272 (R^2 = 0.9918). This indicates that the process is predominantly diffusion-controlled (Ye et al., 2021), suggesting that the electrochemical reaction of EC on the $LaMnO_3$@GO@MIP/GCE electrode is reversible and governed by diffusion.

CV was employed to assess the relationship between the EC concentration and the $LaMnO_3$@GO@MIP/GCE electrochemical sensor. Fig. 4e presents the CV curve of $LaMnO_3$@GO@MIP/GCE in 0.01 M PBS with EC concentrations ranging from 0.4 to 4 mM. At a scanning rate of 50 mV s^{-1}, a sharp oxidation peak was observed at 0.67 5 V and a reduction peak at 0.397 V. Fig. 4f shows the correlation curve between the oxidation peak current difference and the EC concentration, with the linear regression equation given by ΔI (μA) = 0.9463 c(mM) + 2.100 5 (R^2 = 0.9906). These results demonstrate that various EC concentrations can be effectively oxidized on the surface of $LaMnO_3$@GO@MIP/GCE, indicating the feasibility of preparing a $LaMnO_3$@GO@MIP/GCE sensor for EC detection.

3.4. Quantitative EC detection

The square wave voltammetry (SWV) technique was used to evaluate the detection limit of the $LaMnO_3$@GO@MIP/GCE electrochemical sensor. SWV measurements were recorded for different EC concentrations in 0.01 M PBS at pH 7.5(Fig. 5 a, b). When the EC concentration ranged from 10 to 2000 μM, a two-band linear correlation was observed between ΔI and concentration (c) (Fig. 5c). At low concentrations (10–2 50 μM) of EC, the regression equation was ΔI(μA) = 0.0084c(μM) + 0.10 5 (R^2 = 0.99 5 5), and a sensitivity of 0.119 μA μM^{-1} cm^{-2}. As the concentration range increased to 2 50–2000 μM, the slope of the linear equation decreased to 0.0019. The regression equation was ΔI(μA) = 0.0019c (μM) + 1.7841 (R^2 = 0.998 5), indicating a high level of correlation. The sensitivity of the equation was 0.027 μA μM^{-1} cm^{-2}. The results indicate that the $LaMnO_3$@GO@MIP/GCE sensor exhibits higher sensitivity at lower concentrations, with a slope of 0.0084, likely due to the excellent surface area of the sensor for blot recognition. However, the imprinting cavity is limited, resulting in a significantly lower kinetic adsorption rate at higher concentrations (Ye et al., 2021). The LOD and LOQ of EC were calculated according to the definitions provided by the International Union of Pure and Applied Chemistry (IUPAC) (Zhang et al., 2022):

$$LOD = \frac{3\sigma}{k} \quad (1)$$

$$LOQ = \frac{10\sigma}{k} \quad (2)$$

Where: σ is the standard deviation calculated from the 10 blank sample values, and k is the slope of linear regression over the low

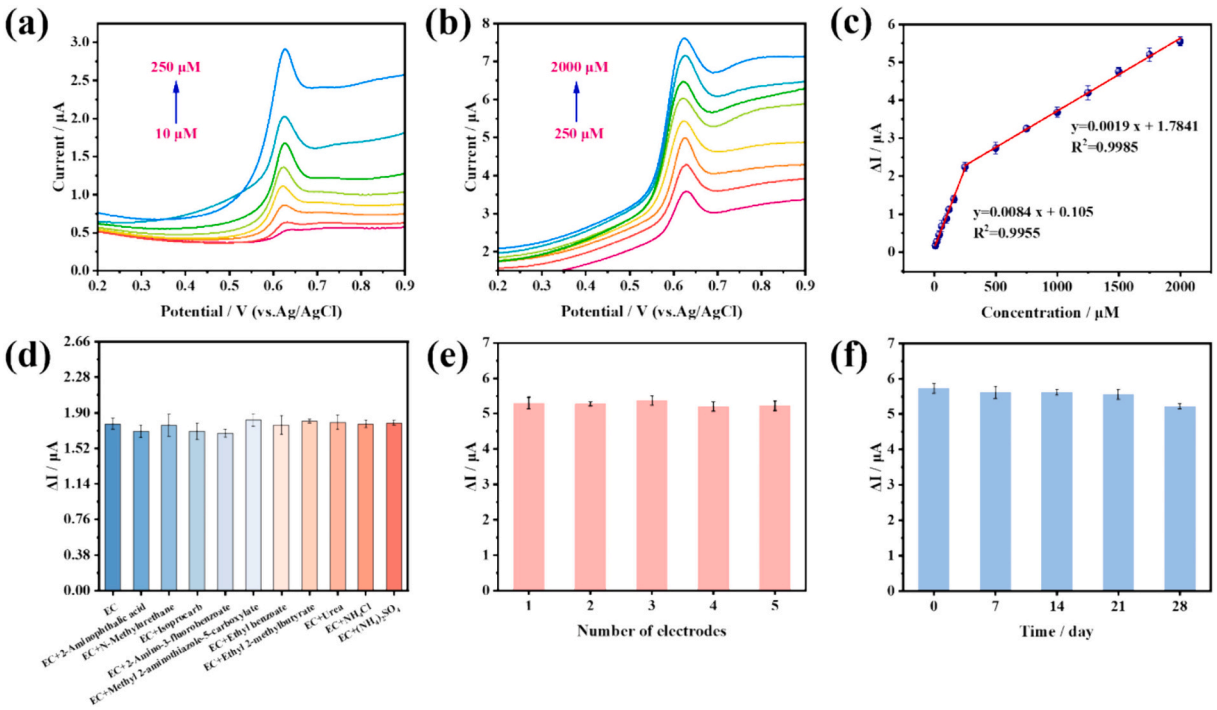

Fig. 5. **(a, b)** SWV curves of $LaMnO_3$@GO@MIP/GCE in 0.01 M PBS (pH = 7.5) with different EC concentrations (10–2000 μM); **(c)** Linear fit of the oxidation peak current difference corresponding to EC concentration; **(d)** Selectivity, **(e)** reproducibility and **(f)** stability ability of $LaMnO_3$@GO@MIP/GCE.

concentration range. The calculated LOD and LOQ are 2.18 μM and 7.26 μM, respectively, with a linear range of 10–2000 μM. Additionally, compared with other published EC detection methods(Table S1), the developed $LaMnO_3$@GO@MIP/GCE sensor is characterized by its simplicity and speed, absence of complex electrode modification materials, and ability to achieve low detection limits with high sensitivity.

3.5. Selectivity, repeatability, and stability of sensors

The selectivity, reusability, and stability of the sensor are crucial factors for expanding the practical application of molecularly imprinted electrochemical sensors. To evaluate the specific selectivity and interference resistance of the modified MIP sensor, we introduced 1 mM of various disruptors, such as 2-aminophthalic acid, *n*-methylurethane, isoprocarb, 2-amino-3-fluorobenzoate, methyl 2-aminothiazole-5-carboxylate, ethyl benzoate, ethyl 2-methylbutyrate, urea, ammonium chloride, and ammonium sulfate, together with similar substances into a 0.01 M PBS solution (pH = 7.5) containing EC at a concentration of 200 μM. The results illustrated in Fig. 5d show that the presence of large concentrations of disruptors did not result in any significant change in the response current ($p > 0.0\,5$), indicating that the modified MIP sensor exhibits excellent selectivity toward EC.

To assess the repeatability of the fabricated electrodes, five $LaMnO_3$@GO@MIP/GCE electrodes were prepared under identical conditions. These electrodes were used to analyze a 1.7 5 mM EC solution (0.01 M PBS, pH = 7.5), as depicted in Fig. 5e. The variation in peak current among these electrodes was found to be insignificant at a significance level of 0.0 5. Additionally, the relative standard deviation (RSD) was 1.20 5%, indicating excellent repeatability of the sensor. The storage durability of the $LaMnO_3$@GO@MIP/GCE sensor was tested over a 28-day storage period at room temperature. The sensor performance was evaluated by measuring the SWV response of a solution containing 1.7 5 mM EC in 0.01 M PBS with a pH of 7.5. The results, shown in Fig. 5f, revealed minimal variation in the intensity of the EC oxidation current at different time intervals. After 28 days, the molecularly imprinted electrochemical sensor retained 91.10% of its initial signal, confirming its high stability, with a RSD of 3.312%. These results confirm the exceptional performance of the modified electrode. The $LaMnO_3$@GO@MIP/GCE sensor has promising potential for practical applications.

3.6. Actual sample analysis

To further assess the practical application of the developed sensor, the $LaMnO_3$@GO@MIP/GCE sensor was used to detect EC in Baijiu samples. The recovery rate was determined using the standard addition method, and the results are summarized in Table S1. The recovery rates ranged from 93.12% to 99.80%, with a repeatability RSD of less than 5%. Additionally, real samples containing EC were analyzed, and the detection data were validated using the GC–MS technique. The quantitative EC results obtained by $LaMnO_3$@GO@MIP/GCE closely matched those obtained by GC–MS, indicating that this sensor is a reliable tool for determining EC in real samples.

4. Conclusions

In summary, we propose a simple sol-gel method for fixing the perovskite compound lanthanum manganate on GO. This is the first study in which lanthanum manganate combined with GO was used to enhance the performance of molecularly imprinted sensors. The three-dimensional nanostructure of lanthanum manganate offers abundant reaction sites, facilitating the rapid identification and detection of EC. GO ensures efficient conduction and amplification of electrochemical signals because of its high specific surface area and excellent electrical conductivity. The optimized conditions demonstrated a robust linear relationship between the oxidation peak current difference and the EC concentration, ranging from 10 to 2000 μM, with a detection limit of 2.18 μM. The sensor achieved detection recovery rates for EC in Baijiu between 93.12% and 99.80%, which was marked by good reproducibility and minimal interference, making it a practical platform for EC detection in Baijiu. The $LaMnO_3$@GO@MIP/GCE sensor outperforms many existing biosensors in terms of cost, stability, and operating

conditions, making it highly suitable for practical EC detection applications. In the future, this sensing method is expected to be widely adopted across various food and beverage applications, providing a reliable and efficient solution for food safety inspection.

Funding

This work was supported by the Scientific Research and Innovation Team Program of Sichuan University of Science and Engineering; Wuliangye Group research project (CXY2020ZR004).

CRediT authorship contribution statement

Wanqi Zheng: Writing – review & editing, Writing – original draft, Software. **Mingcai Yao:** Methodology, Formal analysis. **Yinjiang Leng:** Visualization. **Kangjie Yu:** Conceptualization. **Xiongjun Xiao:** Formal analysis. **Huiling Huang:** Investigation. **Xiao Yu:** Data curation. **Yi Ma:** Supervision, Project administration, Funding acquisition. **Changjun Hou:** Writing – review & editing, Supervision, Project administration.

Declaration of competing interest

The authors declare that they have no known competing financial interests or personal relationships that could have appeared to influence the work reported in this paper.

Data availability

The data that has been used is confidential.

Appendix A. Supplementary data

Supplementary data to this article can be found online at https://doi.org/10.1016/j.fochx.2024.101752.

References

Aguilera Ojeda, D. A., Wrobel, K., Corrales Escobosa, A. R., Mejia Diaz, L. F., & Wrobel, K. (2019). Automated pre-column derivatization with 9-xanthydrol for the determination of ethyl carbamate in food matrices by high performance liquid chromatography with fluorimetric detection. *Journal of Food Measurement and Characterization, 13*, 2722–2728. https://doi.org/10.1007/s11694-019-00193-6

Balaji, A., Yang, S., Wang, J., & Zhang, J. (2019). Graphene oxide-based nanostructured DNA sensor. *Biosensors, 9*(2), 74. https://doi.org/10.3390/bios9020074

Chen, X., Qu, Z., Xie, M., Zhang, M., Ai, J., Ren, G., & Yang, Y. (2024). In-situ crosslinking reaction of graphene oxide & waterborne epoxy resin to construct continuous phase anticorrosive coating. *Arabian Journal of Chemistry, 17*(6), Article 105795. https://doi.org/10.1016/j.arabjc.2024.105795

Deng, H., Ji, L., Han, X., Wu, T., Han, B., Li, C., & You, Y. (2023). Research progress on the application of different controlling strategies to minimizing ethyl carbamate in grape wine. *Comprehensive Reviews in Food Science and Food Safety, 22*(3), 1495–1516. https://doi.org/10.1111/1541-4337.13119

Deshmukh, V. V., Harini, H. V., Nagaswarupa, H. P., Naik, R., & Ravikumar, C. R. (2023). Development of novel Co^{3+} doped $LaMnO_3$ perovskite electrodes for supercapacitors and sensors: Mechanism of electrochemical energy storage and oxygen intercalation. *Journal of Energy Storage, 68*, Article 107805. https://doi.org/10.1016/j.est.2023.107805

Elhachem, M., Bou-Maroun, E., Abboud, M., Cayot, P., & Maroun, R. G. (2023). Optimization of a molecularly imprinted polymer synthesis for a rapid detection of Caffeic acid in wine. *Foods, 12*(8), 1660. https://doi.org/10.3390/foods12081660

Fu, H. J., Chen, Z. J., Wang, H., Luo, L., Wang, Y., Huang, R. M., & Hammock, B. (2021). Development of a sensitive non-competitive immunoassay via immunocomplex binding peptide for the determination of ethyl carbamate in wine samples. *Journal of Hazardous Materials, 406*, Article 124288. https://doi.org/10.1016/j.jhazmat.2020.124288

Fu, K., Zhang, R., He, J., Bai, H., & Zhang, G. (2019). Sensitive detection of ketamine with an electrochemical sensor based on UV-induced polymerized molecularly imprinted membranes at graphene and MOFs modified electrode. *Biosensors and Bioelectronics, 143*, Article 111636. https://doi.org/10.1016/j.bios.2019.111636

George, K. J., Halali, V. V. C. G. S., Suvina, V., Sakar, M., & Balakrishna, R. G. (2020). Perovskite nanomaterials as optical and electrochemical sensors. *Inorganic Chemistry Frontiers, 7*(14), 2702–2725. https://doi.org/10.1039/d0qi00306a

Guo, M., Zhang, X., Zheng, Y., & Huang, D. (2018). Synthesis of switchable intelligent molecularly imprinted polymers with selective adsorption of ethyl carbamate and their application in electrochemical sensor analysis. *RSC Advances, 8*(45), 25636–25644. https://doi.org/10.1039/c8ra04323j

Han, L., Meng, C., Zhang, D., Liu, H., & Sun, B. (2022). Fabrication of a fluorescence probe via molecularly imprinted polymers on carbazole-based covalent organic frameworks for optosensing of ethyl carbamate in fermented alcoholic beverages. *Analytica Chimica Acta, 1192*, Article 339381. https://doi.org/10.1016/j.aca.2021.339381

Han, L., Zhu, X., Zhang, D., Liu, H., & Sun, B. (2023). Peptide-based molecularly imprinted polymer: A visual and digital platform for specific recognition and detection of ethyl carbamate. *ACS Sensors, 8*(2), 694–703. https://doi.org/10.1021/acssensors.2c02197

Han, Y., Zhang, R., Dong, C., Cheng, F., & Guo, Y. (2019). Sensitive electrochemical sensor for nitrite ions based on rose-like AuNPs/MoS_2/graphene composite. *Biosensors and Bioelectronics, 142*, Article 111529. https://doi.org/10.1016/j.bios.2019.111529

Koventhan, C., Shanmugam, R., & Chen, S. M. (2023). Development of highly sensitive electrochemical sensor for antipsychotic drug perphenazine using perovskite structured lanthanum cobalt oxide nanoparticles wrapped graphitic carbon nitride nanocomposites. *Electrochimica Acta, 467*, Article 143096. https://doi.org/10.1016/j.electacta.2023.143096

Lai, H., Ming, P., Wu, M., Wang, S., Sun, D., & Zhai, H. (2023). An electrochemical aptasensor based on P-Ce-MOF@MWCNTs as signal amplification strategy for highly sensitive detection of zearalenone. *Food Chemistry, 423*, Article 136331. https://doi.org/10.1016/j.foodchem.2023.136331

Lee, G. H., Bang, D. Y., Lim, J. H., Yoon, S. M., Yea, M. J., & Chi, Y. M. (2017). Simultaneous determination of ethyl carbamate and urea in Korean rice wine by ultra-performance liquid chromatography coupled with mass spectrometric detection. *Journal of Chromatography B, 1065-1066*, 44–49. https://doi.org/10.1016/j.jchromb.2017.09.011

Li, X., Wan, J., Wang, Y., Chi, H., Yan, Z., & Ding, S. (2020). Selective removal and persulfate catalytic decomposition of diethyl phthalate from contaminated water on modified MIL100 through surface molecular imprinting. *Chemosphere, 240*, Article 124875. https://doi.org/10.1016/j.chemosphere.2019.124875

Liang, Y., Yu, L., Yang, R., Li, X., Qu, L., & Li, J. (2017). High sensitive and selective graphene oxide/molecularly imprinted polymer electrochemical sensor for 2,4-dichlorophenol in water. *Sensors and Actuators B: Chemical, 240*, 1330–1335. https://doi.org/10.1016/j.snb.2016.08.137

Luo, L., Song, Y., Zhu, C., Fu, S., Shi, Q., Sun, Y. M., & Lin, Y. (2018). Fluorescent silicon nanoparticles-based ratiometric fluorescence immunoassay for sensitive detection of ethyl carbamate in red wine. *Sensors and Actuators B: Chemical, 255*, 2742–2749. https://doi.org/10.1016/j.snb.2017.09.088

Ma, Y., Leng, Y., Huo, D., Zhao, D., Zheng, J., Yang, H., & Hou, C. (2023). A sensitive enzyme-free electrochemical sensor based on a rod-shaped bimetallic MOF anchored on graphene oxide nanosheets for determination of glucose in huangshui. *Analytical Methods, 15*(20), 2417–2426. https://doi.org/10.1039/d2ay01977a

Ma, Z., Zhao, T., Cui, S., Zhao, X., Fan, Y., & Song, J. (2022). Determination of ethyl carbamate in wine by matrix modification-assisted headspace single-drop microextraction and gas chromatography–mass spectrometry technique. *Food Chemistry, 373*, Article 131573. https://doi.org/10.1016/j.foodchem.2021.131573

Mani, A., Rajeev, M. R., & Anirudhan, T. S. (2023). Silver decorated silanized graphene oxide based molecularly surface imprinted electrochemical sensor for the trace level detection of L- tryptophan. *Materials Chemistry and Physics, 299*, Article 127445. https://doi.org/10.1016/j.matchemphys.2023.127445

Meng, C., Liu, H., & Sun, B. (2024). Molecularly imprinted polymers: A new solution for controlling ethyl carbamate in fermented alcoholic beverages. *Separation & Purification Reviews*, 1–20. https://doi.org/10.1080/15422119.2024.2339851

Mintz Hemed, N., Leal-Ortiz, S., Zhao, E. T., & Melosh, N. A. (2023). On-demand, reversible, ultrasensitive polymer membrane based on molecular imprinting polymer. *ACS Nano, 17*(6), 5632–5643. https://doi.org/10.1021/acsnano.2c11618

Mohseni, S. N., Majidi, M. R., Sohrabi, H., Mahmoudi, E., Caylak Delibas, N., & Niaei, A. (2024). High-throughput screening of perovskite-based electrochemical sensor for determination of piroxicam via electrocatalytic oxidation in pharmaceutical and biomedical analysis. *Materials Chemistry and Physics, 316*, Article 129100. https://doi.org/10.1016/j.matchemphys.2024.129100

Qi, H., Chen, H., Wang, Y., & Jiang, L. (2018). Detection of ethyl carbamate in liquors using surface-enhanced Raman spectroscopy. *Royal Society Open Science, 5*(12), Article 181539. https://doi.org/10.1098/rsos.181539

Scheller, F. W., Zhang, X., Yarman, A., Wollenberger, U., & Gyurcsányi, R. E. (2019). Molecularly imprinted polymer-based electrochemical sensors for biopolymers. *Current Opinion in Electrochemistry, 14*, 53–59. https://doi.org/10.1016/j.coelec.2018.12.005

Sfirloaga, P., Taranu, B. O., Poienar, M., & Vlazan, P. (2023). Addressing electrocatalytic activity of metal-substituted lanthanum manganite for the hydrogen evolution reaction. *Surfaces and Interfaces, 39*, Article 102881. https://doi.org/10.1016/j.surfin.2023.102881

Shalamitskiy, M. Y., Tanashchuk, T. N., Cherviak, S. N., Vasyagin, E. A., Ravin, N. V., & Mardanov, A. V. (2023). Ethyl carbamate in fermented food products: Sources of appearance, hazards and methods for reducing its content. *Foods, 12*(20), 3816. https://doi.org/10.3390/foods12203816

Song, Y. L., Wang, Z. C., Yan, Y. D., Zhang, M. L., Wang, G. L., Yin, T. Q., & Qiu, M. (2020). Molten salt synthesis and supercapacitor properties of oxygen-vacancy $LaMnO_{3-\delta}$. *Journal of Energy Chemistry, 43*, 173–181. https://doi.org/10.1016/j.jechem.2019.09.007

Tu, Q., Qi, W., Zhao, J., Zhang, L., & Guo, Y. (2018). Quantification ethyl carbamate in wines using reaction-assisted-extraction with 9-xanthydrol and detection by heart-

cutting multidimensional gas chromatography-mass spectrometry. *Analytica Chimica Acta, 1001*, 86–92. https://doi.org/10.1016/j.aca.2017.11.022

Wei, L., Chen, H., Liu, R., Wang, S., Liu, T., Hu, Z., & Fu, H. (2021). Fluorescent sensor based on quantum dots and nano-porphyrin for highly sensitive and specific determination of ethyl carbamate in fermented food. *Journal of the Science of Food and Agriculture, 101*(15), 6193–6201. https://doi.org/10.1002/jsfa.11270

Wu, L., Wang, Y., Zhou, S., Zhu, Y., & Chen, X. (2021). Enzyme-induced cu^{2+}/Cu^{+} conversion as the electrochemical signal for sensitive detection of ethyl carbamate. *Analytica Chimica Acta, 1151*, Article 338256. https://doi.org/10.1016/j.aca.2021.338256

Xia, L., Yang, Y., Yang, H., Tang, Y., Zhou, J., & Wu, Y. (2022). Screening and identification of an aptamer as novel recognition molecule in the test strip and its application for visual detection of ethyl carbamate in liquor. *Analytica Chimica Acta, 1226*, Article 340289. https://doi.org/10.1016/j.aca.2022.340289

Xing, Y., Ding, X., Liang, X., Liu, G., Hou, S., & Hou, S. (2023). Magnetic MXene-based molecularly imprinted electrochemical sensor for methylmalonic acid. *Microchimica Acta, 190*(6), 208. https://doi.org/10.1007/s00604-023-05791-2

Yao, M., Luo, G., Ran, Y., Li, C., & Dong, L. (2024). A sensitive enzyme-free electrochemical sensor based on $ZnWO_4/\gamma$-Fe_2O_3 magnetic molecularly imprinted polymer for specific recognition and determination of chloramphenicol. *Microchemical Journal, 201*, Article 110654. https://doi.org/10.1016/j.microc.2024.110654

Ye, C., Chen, X., Zhang, D., Xu, J., Xi, H., Wu, T., & Huang, G. (2021). Study on the properties and reaction mechanism of polypyrrole@norfloxacin molecularly imprinted electrochemical sensor based on three-dimensional CoFe-MOFs/AuNPs. *Electrochimica Acta, 379*, Article 138174. https://doi.org/10.1016/j.electacta.2021.138174

You, M., Yang, S., Tang, W., Zhang, F., & He, P. (2018). Molecularly imprinted polymers-based electrochemical DNA biosensor for the determination of BRCA-1 amplified by SiO_2@ag. *Biosensors and Bioelectronics, 112*, 72–78. https://doi.org/10.1016/j.bios.2018.04.038

Zhang, H., & Yi, J. (2018). Enhanced ethanol gas sensing performance of ZnO nanoflowers decorated with $LaMnO_3$ perovskite nanoparticles. *Materials Letters, 216*, 196–198. https://doi.org/10.1016/j.matlet.2018.01.018

Zhang, J., Chen, Y., Li, L., Chen, X., An, W., Qian, X., & Tao, Y. (2024). $LaMnO_3/Co_3O_4$ nanocomposite for enhanced triethylamine sensing properties. *Journal of Rare Earths, 42*(4), 733–742. https://doi.org/10.1016/j.jre.2023.05.007

Zhang, L., Yin, M., Wei, X., Sun, Y., Chen, Y., Qi, S., & Xu, D. (2022). Synthesis of rGO@PDA@AuNPs for an effective electrochemical chloramphenicol sensor. *Diamond and Related Materials, 128*, Article 109311. https://doi.org/10.1016/j.diamond.2022.109311

Zhou, K., Patrignani, F., Sun, Y. M., Lanciotti, R., & Xu, Z. L. (2021). Inhibition of ethyl carbamate accumulation in soy sauce by adding quercetin and ornithine during thermal process. *Food Chemistry, 343*, Article 128528. https://doi.org/10.1016/j.foodchem.2020.128528

Zhu, S., Yang, Y., Chen, K., Su, Z., Wang, J., Li, S., & Xie, A. (2022). Novel cubic gravel-like $EDAPbCl_4$@ZIF-67 as electrochemical sensor for the detection of protocatechuic acid. *Journal of Alloys and Compounds, 903*, Article 163946. https://doi.org/10.1016/j.jallcom.2022.163946